Electronic Supplementary Material (ESI) for Chemical Communications

Supporting Information

for

A new "turn-on" chemodosimeter for Hg^{2+}: ICT fluorophore formation via Hg^{2+}-induced carbaldehyde recovery from 1,3-dithiane

Yuncong Chen, Chengcheng Zhu, Zhenghao Yang, Jing Li, Yang Jiao, Weijiang He*, Junjie Chen and Zijian Guo*

State Key Laboratory of Coordination Chemistry, School of chemistry and chemical engineering, Nanjing University, Nanjing 210093, China

Email: heweij69@nju.edu.cn; zguo@nju.edu.cn

1.Materials and general methods.

All the solvents were of analytic grade. The stock solutions of metal ions were prepared from $MnCl_2$, $CoCl_2 \cdot 6H_2O$, $Zn(NO_3)_2 \cdot 7H_2O$, $CaCl_2$, NaCl, $CuSO_4$, $AgNO_3$, $NiCl_2 \cdot 6H_2O$, KCl, $FeCl_2$, $CdCl_2 \cdot 2.5H_2O$, $HgCl_2$, $MgCl_2 \cdot 6H_2O$ with doubly distilled water. The stock solutions of Cu(I) was prepared from $[Cu(MeCN)_4][PF_6]$ in acetonitrile. The ^1H NMR and ^{13}C NMR spectra were recorded on Bruker DRX-500 with TMS as internal standard. Mass spectrometric data were determined with a Bruker Autoflex II MALDI-TOF mass spectrometer. Fluorescence measurements were performed on an AMINCO Bowman series 2 with 8 nm slit for both excitation and emission. Absorption spectra were measured on a Shimadzu UV-3100 or an UV-VIS-NIR spectrophotometer. All pH measurements were determined by a Model PHS-3C meter. All experiments with live animals were performed in compliance with the relevant laws in china and approved by Nanjing University.

2. Synthesis of DT-ABD.

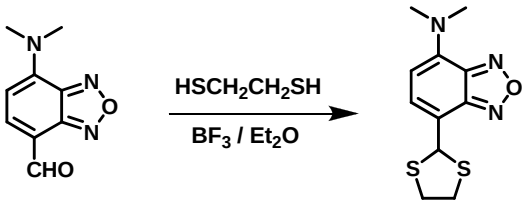

Scheme S1. Synthesis of **DT-ABD**.

To a Et_2O solution (15 mL) containing 573 mg (3.0 mmol) **Al-ABD**, 505 μL (6.0 mmol) of 1,2-ethanedithiol and 184 μL (1.5 mmol) of boron trifluoride etherate were added dropwise with stirring at room temperature for 24 h. Then the solvent was removed via evaporation in vacuo. The residue was dissolved in 20 mL CH_2Cl_2, and the organic layer was washed with water (20 mL×3). Then the organic layer was dried over anhydrous $MgSO_4$. After filtering off the desiccant from the organic layer, the solvent were removed via evaporation in vacuo. Then the the residue was purified by column chromatography (petroleum ether: dichloromethane = 1:3, R_f = 0.35) to afford a red powder (0.653g, 81%). ^1H NMR (500 MHz, $CDCl_3$): δ 3.33 (s, 6H, -N(CH_3)$_2$), 3.38-3.43 (m, 2H, -CH_2), 3.57-3.61 (m, 2H, -CH_2), 6.00 (d, 1H, J = 2.7 Hz, -ArH), 6.07 (s, 1H, -CHS_2), 7.42 (d, 1H, J = 2.7 Hz, -ArH). ^{13}C NMR (125 MHz, $CDCl_3$): δ 39.80, 41.97, 51.88, 104.21, 115.71, 131.06, 139.60, 145.94, 149.15. ESI-MS (m/z): calcd. 268.38, found 268.33 for $[M+H]^+$. Element analysis (%) Calcd. for $C_{11}H_{13}N_3OS_2$: C, 49.41; H, 4.90; N, 15.72. Found: C, 49. 30; H, 5.12 ; N, 15.61.

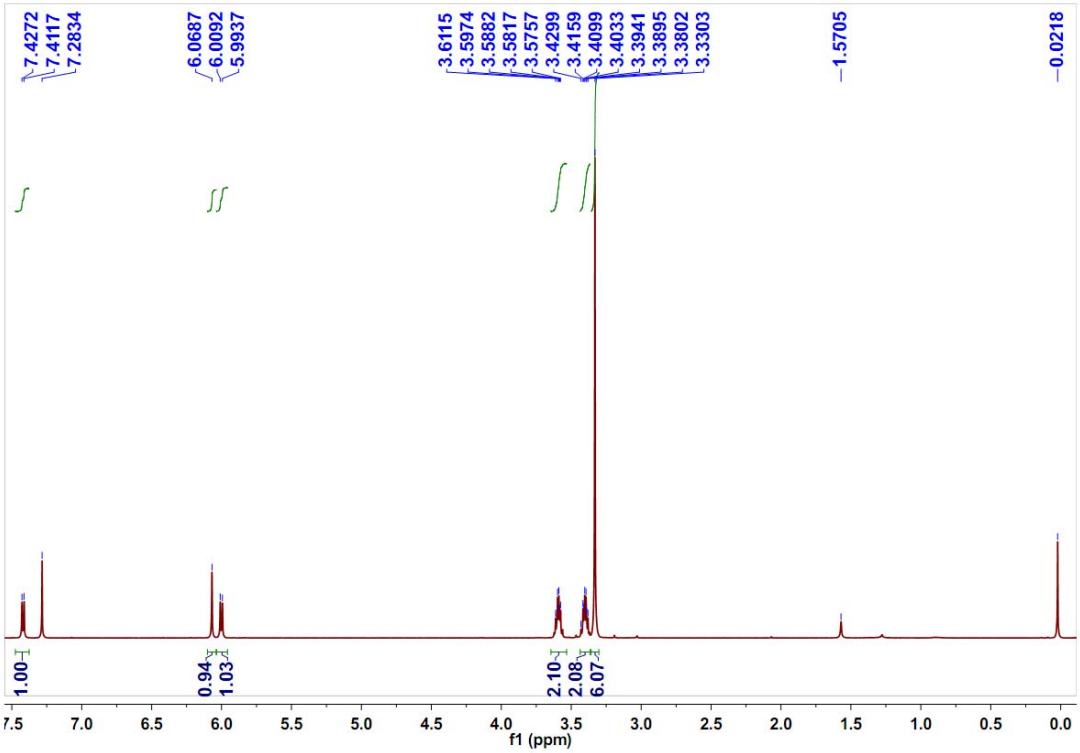

Figure S1. ^{1}H NMR spectrum of **DT-ABD** in $CDCl_3$.

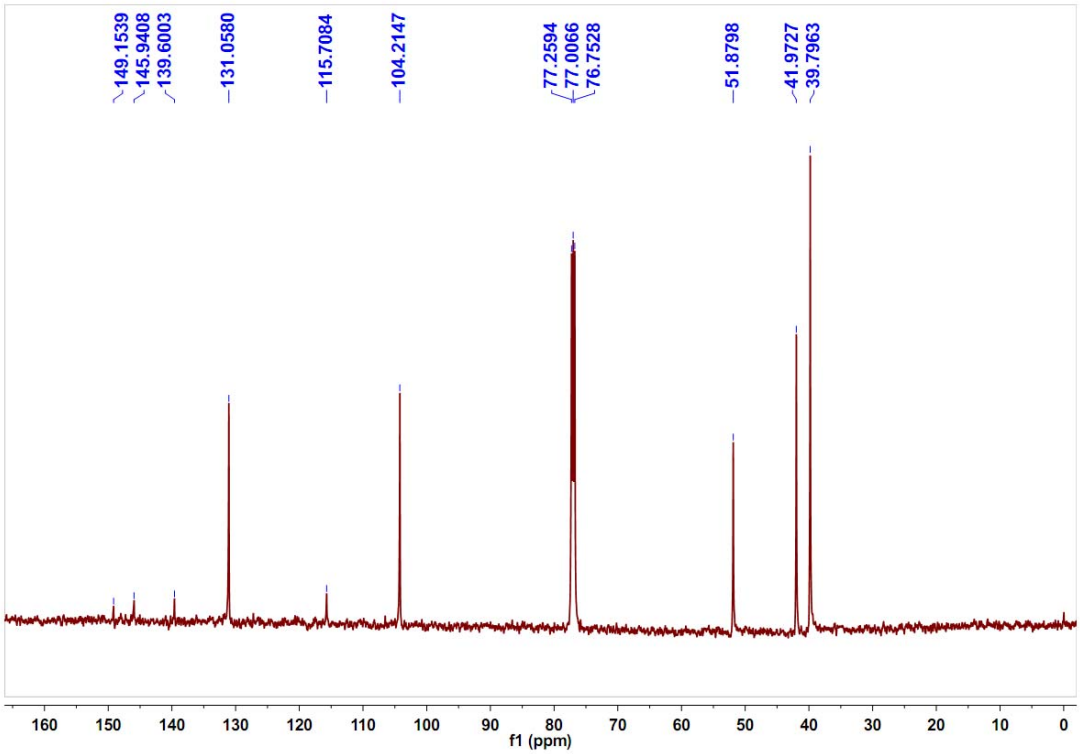

Figure S2. ^{13}C NMR spectrum of **DT-ABD** in $CDCl_3$.

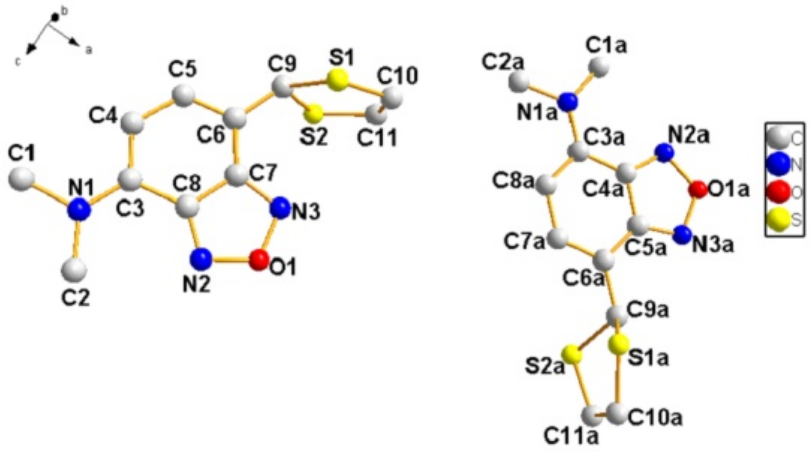

Figure S3. View of crystal structure of **DT-ABD** (H-atoms were omitted for clarity).

Table S1. Crystal parameters and structure refinements for **DT-ABD**

Chemical formula	C11 H13N3OS2
Formula weight	267.36
Temperature (K)	291(2)
Crystal size/mm	0.12*0.10*0.08
Crystal system	Orthorhombic
Space group	Pnma
a/Å	17.6742(11)
b/Å	7.0921(13)
c/Å	19.3659(14)
α(°)	90.00
β(°)	90.00
γ (°)	90.00
V/Å^3	2427.5(5)
Z	8
D_c /g cm^{-3}	1.463
F(000)	1120
θ range (°)	2.10-26.00
Tot., ref. number	12993, 2590
Limiting indices	-19 ≤h ≤ 21, -8 ≤ k ≤ 8, -23≤ l ≤ 19
Observed data [$I > 2\sigma(I)$]	1941
$R_{(int)}$	0.065
R_1,wR_2 [$I > 2\sigma(I)$]	0.0581, 0.1510
GOF on F^2	1.046
S	1.046

Table S2. Selected bond lengths (Å) and angles (°) for **DT-ABD**.

Bond lengths (Å)		Bond angles (°)	
C(9)-S(1)	1.834(3)	C(1)-N(1)-C(3)	126.4(4)
C(9)-S(2)	1.834(3)	C(6)-C(9)-S(1)	112.90(16)
S(1)-C(10)	1.689(4)	C(9)-S(1)-C(10)	100.43(19)
S(2)-C(11)	1.689(4)	S(1a)-C(9a)-S(2a)	105.5(2)
N(1)-C(3)	1.354(6)	N(2)-O(1)-N(3)	112.5(3)
C(6)-C(9)	1.483(8)	C(8)-N(2)-O(1)	105.1(3)
C(10)-C(11)	1.512(5)	C(1)-N(1)-C(2)	114.7(4)
C(1)-N(1)	1.418(6)	C(6a)-C(9a)-S(1a)	112.90(16)
C(2)-N(1)	1.418(6)	C(9a)-S(1a)-C(10a)	95.00(16)

3. Temporal tracking of DT-ABD fluorescence upon Hg^{2+} addition.

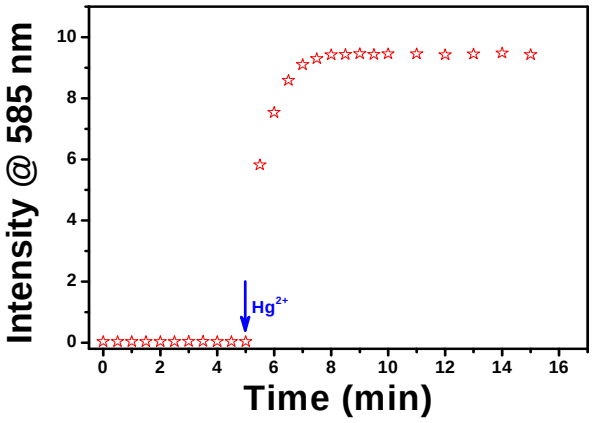

Figure S4. Temporal fluorescence profile of 5 μM **DT-ABD** in HEPES buffer (CH_3CN:H_2O=1:4, pH=7.4) at 585 nm upon the addition of 2 equiv Hg^{2+} at 5^{th} min. Excited at 455 nm.

4. Colorimetric response of DT-ABD to different metal cations.

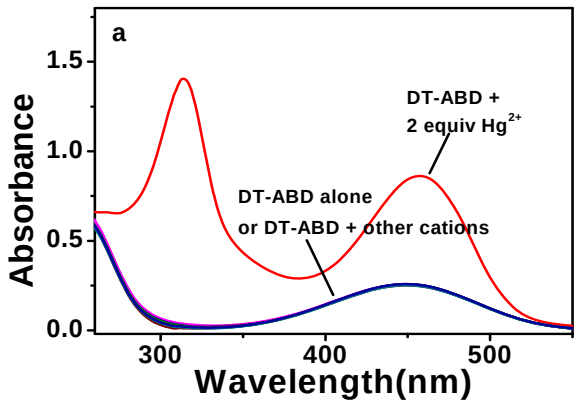

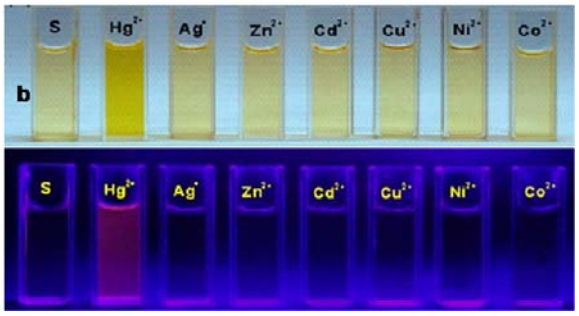

Figure S5. (a) Absorption spectra of 50 μM **DT-ABD** in HEPES buffer (HEPES 50 mM, KNO_3 100 mM, CH_3CN:H_2O = 1:4, pH = 7.40) in the absence and presence of different metal ions. Hg^{2+}: 100 μM, other metal ions: 1000 μM. (b) Colorimetric (upper row) and fluorometric (lower row, irradiated at 365 nm) photographs of **DT-ABD** (50 μM) in the same HEPES buffer with the presence of 2 equiv Hg^{2+} or 20 equiv other metal cations.

5. Detection limit and linear range of DT-ABD for Hg^{2+} detection.

The spectrum of free **DT-ABD** (5 μM, HEPES 50 mM, KNO_3 100 mM, CH_3CN:H_2O = 1:4, pH = 7.40) was collected for 20 times to determine the background noise σ. Then the solution was treated with various concentration of Hg^{2+} from 0.01-5.0 μM, and all fluorescence spectra were collected after mixing for 3 min. A linear regression curve was then fitted according to the emission intensity at 585 nm in the range of 0.01-5.0 μM. As exhibited in Figure S3, **DT-ABD** can quantitatively detect Hg^{2+} in the range from 0.01 to 5.0 μM with good linearity (R^2 = 0.99761).

Another linear regression curve was then fitted according to the data in the range of [Hg^{2+}] from 0.01 to 0.10 μM, and the slope of the curve was obtained (Figure S4). The detection limit (3σ slope^{-1}) was then determined to be 4 nM.

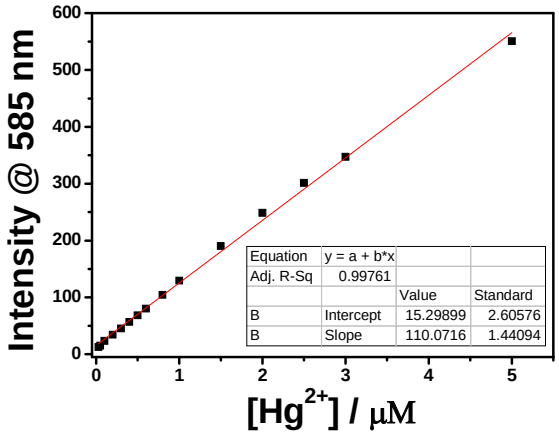

Figure S6. Plot of fluorescence intensity of **DT-ABD** (5 μM) in HEPES buffer (HEPES 50 mM, KNO_3 100 mM, CH_3CN:H_2O = 1:4, pH = 7.40) at 585 nm as a function of the Hg^{2+} concentration in the range of 0.01 –5.0 μM.

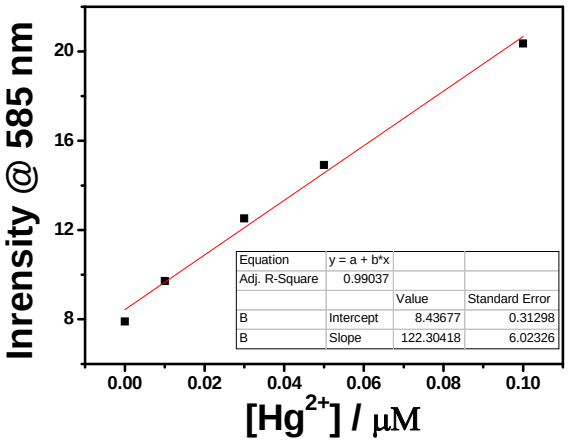

Figure S7. Plot of fluorescence intensity of **DT-ABD** (5 μM) in HEPES buffer (HEPES 50 mM, KNO_3 100 mM, $CH_3CN:H_2O$ = 1:4, pH = 7.40) at 585 nm as a function of the Hg^{2+} concentration in the range of 0.01 –0.10 μM.

6. pH-dependence of DT-ABD sensing ability to Hg^{2+}

pH values of **DT-ABD** solutions (5 μM, $CH_3CN:H_2O$ = 1:4) were adjusted by KOH and HNO_3 solutions. The fluorescence spectra of each solution were collected in a 3 mL cuvette. After mixing with 2 equiv Hg^{2+} for 3 min, the fluorescence spectra were determined again. The pH-dependence was estimated according to the emission intensity at 585 nm.

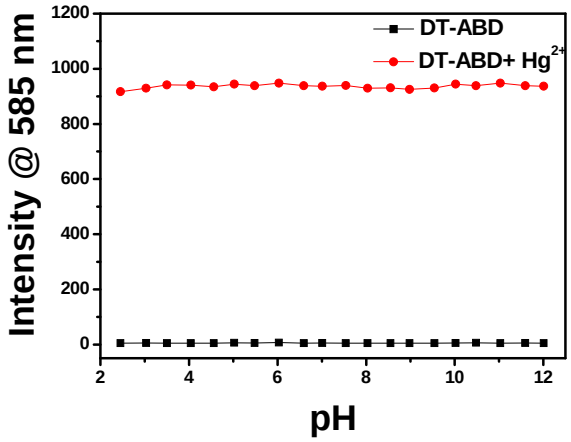

Figure S8. Emission intensity of **DT-ABD** (5 μM, $CH_3CN:H_2O$ = 1:4) at 585 nm at different pH (excited at 455 nm) in the absence or presence of 2 equiv Hg^{2+}.

7. Sensing mechanism study

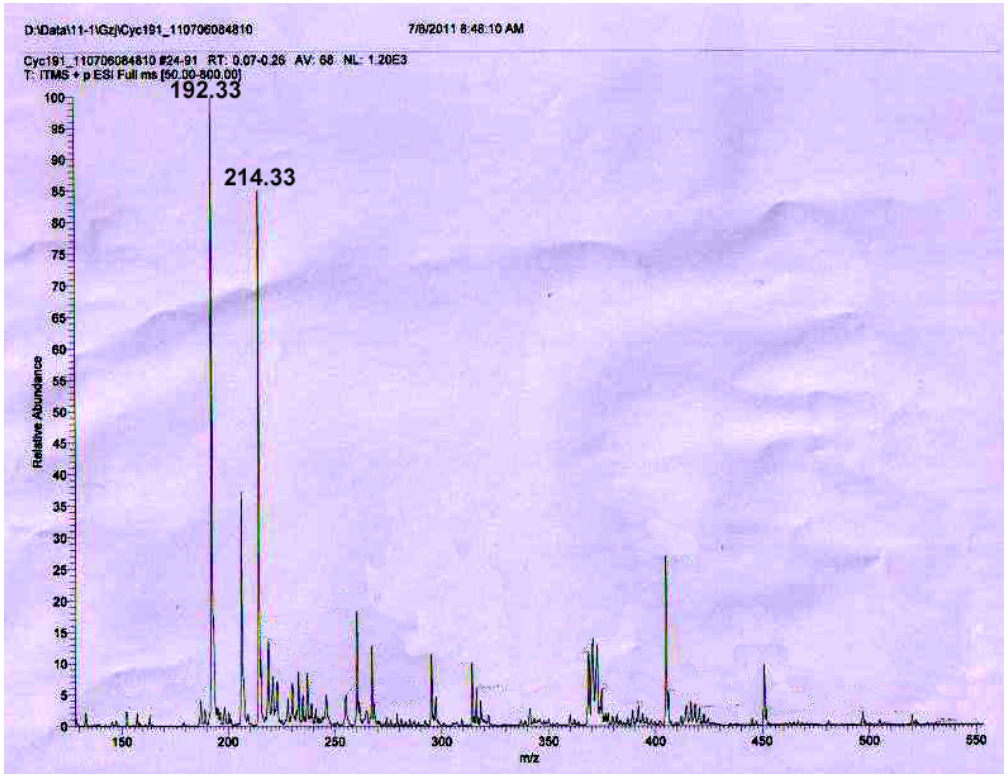

Figure S9. ESI-MS spectrum of **DT-ABD**/Hg^{2+} mixture.

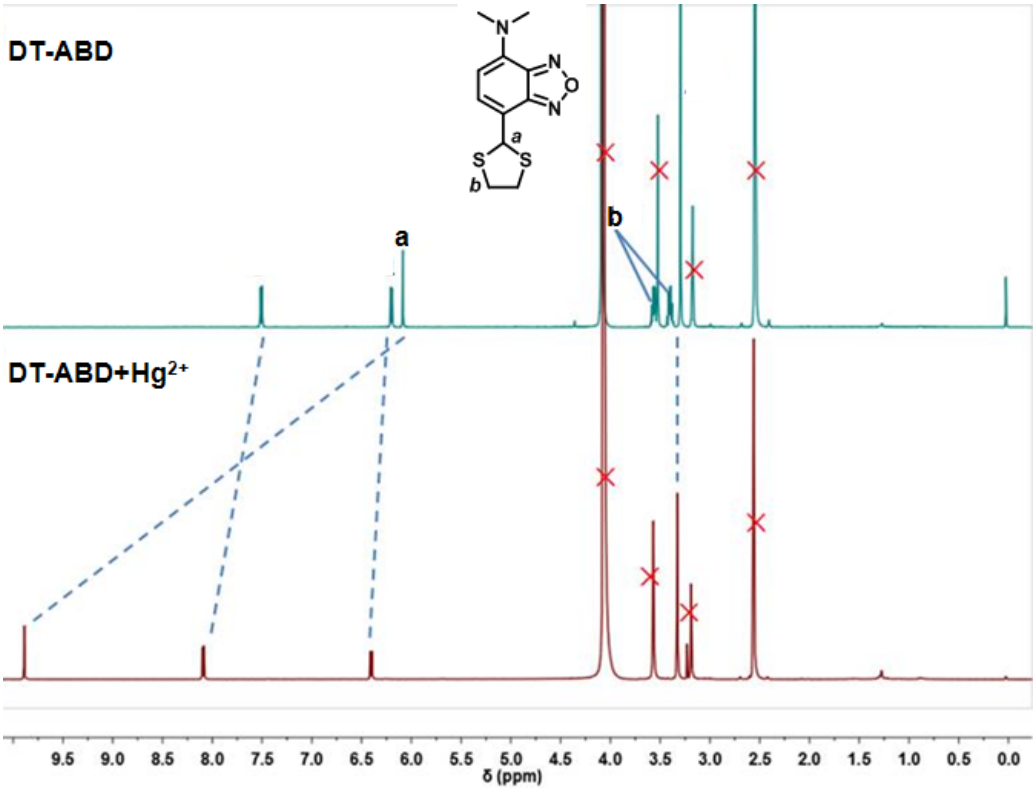

Figure S10. ^{1}H NMR spectra of **DT-ABD** (initial c = 20 mM) in d_6-DMSO/CD_3OD (4:1) obtained upon Hg^{2+} titration (c = 1 M in CD_3OD). The signals labeled with "×" were assigned as signals for solvents and residual H_2O.

8. In vivo Hg^{2+} imaging in zebrafish larvae

The 5-day-old zebrafish larvae were incubated with 10 μM **DT-ABD** in distilled water for 20 min

at 28°C. After washing with distilled water to remove the sensor, the larvae were further incubated with 1 μM $HgCl_2$ for 20 min at 28°C. The zebrafish larvae with or without Hg^{2+} incubation were imaged respectively by both fluorescence microscope (Olympus TH4-200) and laser scanning confocal fluorescence microscope (Zeiss LSM710).

The video file has been submitted as a separated file.

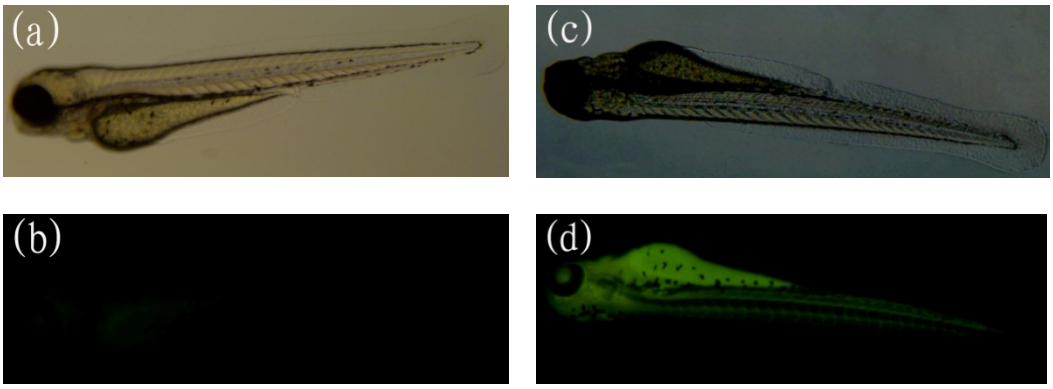

Figure S11. Fluorescence imaging of 5-day-old zebrafish larva treated with 10 μM **DT-ABD** (20 min) at 28ºC. (a) Bright-field image of larva without Hg^{2+} incubation mercury ion. (b) Fluorescence image of zebrafish larva in (a). (c) Bright-field image of zebrafish larva treated with the followed Hg^{2+} incubation (1 μM, 20 min) at 28ºC. (d) Fluorescence image of zebrafish larva in (c).

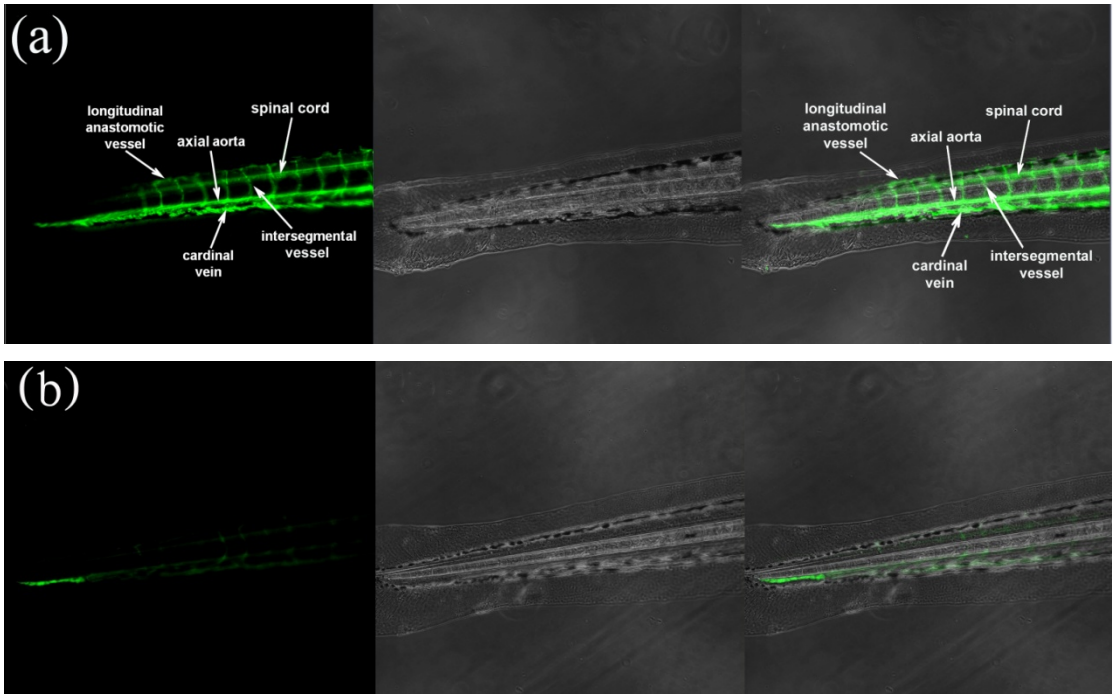

Figure S12. Laser scanning confocal fluorescence imaging of the tail of 5-day-old zebrafish larva treated by 10 μM **DT-ABD** (20 min) with (**a**) or without (**b**) the followed 20 min incubation with 1 μM Hg^{2+}. Left: fluorescence image; middle: bright field image; right: merge of the fluorescence image and bright-field image.

9. Determination of quantum yield.

Fluorescence quantum yield of **Al-ABD** was determined in pure acetonitrile with 4-methylamino-7-nitro-2,1, 3-benzoxadiazole (Φ = 0.38, λ_{ex}=458 nm) as a reference. The quantum yields were calculated using Eq.1:

$$\Phi_u = [(A_s F_u n^2)/ (A_u F_s n_0^2)]\Phi_s. \qquad \text{(Eq.1)}$$

Where A_s and A_u are the absorbance of the reference and sample solution at the reference excitation wavelength, F_s and F_u are the corresponding integrated fluorescence intensity, and n and n_0 are the solvent refractive indexes of sample and reference, respectively. Absorbance of samples and references at their respective excitation wavelengths was controlled to be lower than 0.05.

10. The video of in vivo Hg^{2+} imaging on zebrafish larva was offered as a separated file.